

# Strain and mechanical behavior measurements of soft tissues with digital speckle method

J. Zhang

G. C. Jin

L. B. Meng

L. H. Jian

Tsinghua University  
Department of Engineering Mechanics  
100084, Beijing, China  
E-mail: jun\_zhang00@yahoo.com

A. Y. Wang

S. B. Lu

General Hospital of Chinese PLA  
Institute of Orthopaedics  
100853, Beijing, China

**Abstract.** Soft tissues of the body are composite, typically being made up of collagen and elastin fibers with high water contents. The strain measurement in soft tissues has proven to be a difficult task. The digital speckle method, combined with the image processing technique, has many advantages such as full field, noncontact, and real time. We focus on the use of an improved digital speckle correlation method (DSCM) and time-sequence electric speckle pattern interferometry (TSESPI) to noninvasively obtain continual strain measurements on cartilage and vessel tissues. Monoaxial tensile experiments are well designed and performed under constant temperature and the necessary humidity with smart sensors. Mechanical behaviors such as the tensile modulus and Poisson ratio of specimens are extracted based on the deformation information. A comparison of the advantages and the disadvantages of these techniques as well as some problems concerning strain measurements in soft tissues are also discussed. © 2005 Society of Photo-Optical Instrumentation Engineers. [DOI: 10.1117/1.1895185]

Keywords: soft tissue; digital speckle correlation method; electric speckle pattern interferometry; time sequence; smart sensor.

Paper 03023 received Mar. 4, 2004; revised manuscript received Jun. 2, 2004; accepted for publication Aug. 17, 2004; published online Jun. 14, 2005.

## 1 Introduction

Due to the complexity of biological systems as well as the lack of knowledge about biomaterials, the experimental approach to obtaining biomechanical behaviors of soft tissues is essential.<sup>1-3</sup> Until now, many different techniques have been proposed.<sup>4-7</sup> To avoid interfering with the strain to be measured, most optical methods such as x rays,<sup>8,9</sup> photography,<sup>10,11</sup> video dimension analysis,<sup>12,13</sup> and holography<sup>14</sup> have aimed at being noncontact and noninvasive in the strain measurement of soft tissues. However, few of them can be employed for measuring the displacement and the strain in both a full field and real time, with none of the techniques being widely accepted.<sup>15</sup> In addition, to the *in vitro* experiment itself, the following factors can be significant, including the preparation and storage of the specimen,<sup>16,17</sup> temperature and humidity,<sup>18,19</sup> and the experiment setup.<sup>20</sup> The strain measurement of living tissues has been proven to be difficult.

Digital speckle methods, unlike many optical methods that aim at the strain measurement only based on marked points or dye lines, can be used to determine the deformation with a full field. However, when using speckle techniques, additional problems posed by the deformation of specimen are noteworthy. First, the large displacement with internal strains may lead to speckle decorrelation or poor tracking. Second, the tracking of full-field displacements greatly depends on the quality of speckle patterns on the surface of soft tissues under either white light or a laser. Third, static deformation must be

maintained to keep the specimen to be held stationary and enable plane imaging to satisfy the plane-strain state.

The obvious advantages of the digital speckle correlation method (DSCM), such as the applications of direct surface texture, the variable measuring sensitivity, and the autoremovable rigid-body movement, provide its suitability in the strain measurement of a biological sample. Based on this technique, speckle patterns can be obtained under white light illumination, and the heavy dependence on the test environment is then reduced. Compared to DSCM, traditional electronic speckle pattern interferometry (ESPI) extracts the deformation through fringe patterns generated by laser interference. It can provide complete spatial information with the possibility of contiguous temporal information, and such data are absolute and do not require any form of calibration since the fringe spacing is a function of the defined and stable laser wavelength. Nevertheless, the high cost of computation by DSCM is still a problem, and the interpretation of fringe patterns in ESPI has proved to be a difficult and arduous task. All these disadvantages bring difficulties for realizing the real-time measurement.

The purpose of this paper is to report the applications of two speckle methods in the noninvasive and real-time strain measurements for extracting the full field and dynamic deformation of soft tissues. Experiments are performed under quasistatic loading to maintain the static deformation. Smart sensors and antivibration tables are used to improve the sensitivity and reduce the negative impact on the accuracy by

Address all correspondence to Dr. Jun Zhang, Tsinghua University, Department of Engineering Mechanics, 100084, Beijing, China.

vibration and air turbulence. Speckle size is controlled to some extent by varying the aperture of the observing system. Based on a series of instantaneous speckle patterns captured in sequence, an improved gradient-based DSCM is introduced in cartilage measurement to obtain strains of every state by simply calculating the relative displacement between two successive states without the “pixel-level” tracking and the “absolute displacement” solving. The detection speed is increased sufficiently and the poor tracking for large displacement is therefore avoided. In addition, a time-sequence ESPI (TSESPI) technique with the phase unwrapped only in the time domain is used in the vessel tissue measurement, which is capable of quantitatively measuring continual deformation simply utilizing a conventional ESPI system without phase shifting or a carrier. Based on an automated computer-aided specklegram system, the relatively low costs of the two methods enabled the strain measurement to become an automatic, high-speed, and real-time process.

## 2 Method

Theories of DSCM and ESPI have been well developed and are widely used in many studies.<sup>21–26</sup> In this paper, a gradient-

based DSCM technique<sup>27</sup> and the TSESPI method are introduced in Secs. 2.1 and 2.2 for strain measurements of cartilage tissue (Sec. 3.1) and vessel tissue (Sec. 3.2), respectively. Strains are derived from displacement functions.

### 2.1 Gradient-Based DSCM

The basic principle of DSCM is to match two speckle patterns before and after deformation. The displacement relationship is assumed as following:

$$\mathbf{r}^* = \mathbf{r} + \mathbf{D}(\mathbf{r}) + \mathbf{d}(\mathbf{r}), \quad (1)$$

where  $\mathbf{D}(\mathbf{r})$  is the integer-pixel displacement vector from  $\mathbf{r} = (x, y)^T$  in the initial image  $f(\mathbf{r})$  to  $\mathbf{r}^* = (x^*, y^*)^T$  of the target image  $g(\mathbf{r}^*)$ , and  $\mathbf{d}(\mathbf{r})$  are the corresponding subpixel displacements.

The speckle pattern is characterized by a random intensity distribution that may be described by statistical means. Defining  $\Pi$  as the cross-correlation functional with the first-order Taylor expansions of  $g(\mathbf{r}^*)$  after neglecting high-order terms, and setting  $\mathbf{D}(\mathbf{r})$  to be zero in the subpixel registration, we have

$$\Pi(\mathbf{d}) = \frac{(\sum_{\mathbf{r} \in \mathbf{S}} \{f(\mathbf{r}) - \bar{f}\} \cdot \{[g(\mathbf{r}) + \nabla g(\mathbf{r}) \cdot \mathbf{d}] - [\bar{g} + \overline{\nabla g(\mathbf{r}) \cdot \mathbf{d}}]\})^2}{\sum_{\mathbf{r} \in \mathbf{S}} [f(\mathbf{r}) - \bar{f}]^2 \cdot \sum_{\mathbf{r} \in \mathbf{S}} \{[g(\mathbf{r}) + \nabla g(\mathbf{r}) \cdot \mathbf{d}] - [\bar{g} + \overline{\nabla g(\mathbf{r}) \cdot \mathbf{d}}]\}^2}, \quad (2)$$

where

$$g(\mathbf{r}^*) = g[\mathbf{r} + \mathbf{D}(\mathbf{r})] + \nabla g[\mathbf{r} + \mathbf{D}(\mathbf{r})] \cdot \mathbf{d},$$

$$\nabla = \left( \frac{\partial}{\partial \mathbf{r}} \right)^T = \left( \frac{\partial}{\partial x} \quad \frac{\partial}{\partial y} \right),$$

and  $\mathbf{S}$  is the given  $M \times N$  subset centered at pixel  $r_0$ .

To the real subpixel displacements  $\mathbf{d}$ , the similarity between  $f(\mathbf{r})$  and  $g(\mathbf{r}^*)$  in the subset region will reach the maximum, that is,

$$\frac{\partial \Pi}{\partial \mathbf{d}} = 0. \quad (3)$$

The solution of Eq. (3) can be obtained by

$$\mathbf{d} = \mathbf{A}^{-1} \mathbf{C}, \quad (4)$$

where  $\mathbf{d}$  is the displacement of the subset center, and  $\mathbf{A}$  and  $\mathbf{C}$  are the constant coefficient matrixes given by

$$\mathbf{A} = \begin{bmatrix} A_{11} & A_{12} \\ A_{21} & A_{22} \end{bmatrix} \quad \text{and} \quad \mathbf{C} = \begin{bmatrix} C_1 \\ C_2 \end{bmatrix}, \quad (5)$$

with

$$A_{11} = \sum_{\mathbf{r} \in \mathbf{S}} (F \cdot G_x) \cdot \sum_{\mathbf{r} \in \mathbf{S}} (G \cdot G_x) - \sum_{\mathbf{r} \in \mathbf{S}} (G_x)^2 \cdot \sum_{\mathbf{r} \in \mathbf{S}} (F \cdot G), \quad (6)$$

$$A_{12} = 2 \sum_{\mathbf{r} \in \mathbf{S}} (F \cdot G_x) \cdot \sum_{\mathbf{r} \in \mathbf{S}} (G \cdot G_y) - \sum_{\mathbf{r} \in \mathbf{S}} (G_x \cdot G_y) \cdot \sum_{\mathbf{r} \in \mathbf{S}} (F \cdot G) - \sum_{\mathbf{r} \in \mathbf{S}} (G \cdot G_x) \cdot \sum_{\mathbf{r} \in \mathbf{S}} (F \cdot G_y), \quad (7)$$

$$A_{21} = 2 \sum_{\mathbf{r} \in \mathbf{S}} (F \cdot G_y) \cdot \sum_{\mathbf{r} \in \mathbf{S}} (G \cdot G_x) - \sum_{\mathbf{r} \in \mathbf{S}} (G_x \cdot G_y) \cdot \sum_{\mathbf{r} \in \mathbf{S}} (F \cdot G) - \sum_{\mathbf{r} \in \mathbf{S}} (G \cdot G_y) \cdot \sum_{\mathbf{r} \in \mathbf{S}} (F \cdot G_x), \quad (8)$$

$$A_{22} = \sum_{\mathbf{r} \in \mathbf{S}} (F \cdot G_y) \cdot \sum_{\mathbf{r} \in \mathbf{S}} (G \cdot G_y) - \sum_{\mathbf{r} \in \mathbf{S}} (G_y)^2 \cdot \sum_{\mathbf{r} \in \mathbf{S}} (F \cdot G), \quad (9)$$

$$C_1 = \sum_{\mathbf{r} \in \mathbf{S}} (G \cdot G_x) \cdot \sum_{\mathbf{r} \in \mathbf{S}} (F \cdot G) - \sum_{\mathbf{r} \in \mathbf{S}} (F \cdot G_x) \cdot \sum_{\mathbf{r} \in \mathbf{S}} (G)^2, \quad (10)$$

$$C_2 = \sum_{\mathbf{r} \in \mathbf{S}} (G \cdot G_y) \cdot \sum_{\mathbf{r} \in \mathbf{S}} (F \cdot G) - \sum_{\mathbf{r} \in \mathbf{S}} (F \cdot G_y) \cdot \sum_{\mathbf{r} \in \mathbf{S}} (G)^2, \quad (11)$$

where  $F(\mathbf{r}) = f(\mathbf{r}) - \bar{f}$ ;  $G(\mathbf{r}) = g(\mathbf{r}) - \bar{g}$ ;  $G_x(\mathbf{r}) = g_x(\mathbf{r}) - \bar{g}_x$ ;  $G_y(\mathbf{r}) = g_y(\mathbf{r}) - \bar{g}_y$ ; and  $\bar{f}$ ,  $\bar{g}$ ,  $\bar{g}_x$ , and  $\bar{g}_y$ , are the ensemble average.

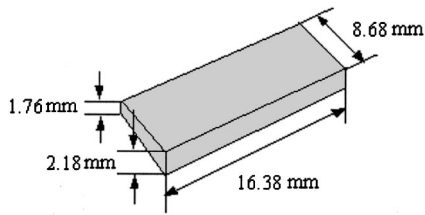


Fig. 1 Specimen dimension between clamps.

Based on the displacement field, the strain field  $\mathbf{E}(\mathbf{r})$  can be determined by

$$\mathbf{E}(\mathbf{r}) = \nabla[\mathbf{D}(\mathbf{r}) + \mathbf{d}(\mathbf{r})], \quad (12)$$

where  $\mathbf{E}(\mathbf{r})$  is a matrix vector and defined as

$$\mathbf{E}(\mathbf{r}) = \begin{bmatrix} \partial u / \partial x & \partial u / \partial y \\ \partial v / \partial x & \partial v / \partial y \end{bmatrix}.$$

### 2.2 Time-Sequence ESPI

For the in-plane displacement measurement, two parallel laser beams illuminate the measuring object symmetrically. In the tiny time intervals  $\Delta t$  during the continuous loading period, the changes of the amplitudes of two beams are quite slow compared with the phase function  $\phi(x, y, t)$ , therefore, the effect of time factor can be omitted. After the object deformed, the interfering intensity  $I'$  can be rewritten as

$$I'(x, y, t) = I_0(x, y) + I_m(x, y) \cos \phi(x, y, t), \quad (13)$$

where  $I_0$  and  $I_m$  are the average intensity and the modulation factor of the temporal speckle interference pattern, respectively; and  $\phi(x, y, t)$  is the time-dependent phase function and defined as

$$\phi(x, y, t) = \phi_1(x, y, t) - \phi_2(x, y, t). \quad (14)$$

With the series temporal speckle patterns captured by CCD, the phase maps can be unwrapped in time domain through scanning the intensity fluctuations of interference patterns and calculating both the average intensity and the modulation. For simplicity, the results are given as follows:

$$\phi(x, y, t_0) = \arccos \left[ \frac{I'(x, y, t_0) - I_0(x, y)}{I_m(x, y)} \right], \quad (15)$$

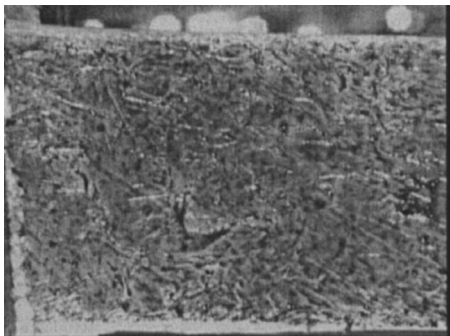


Fig. 2 Specimen surface with speckle pattern.

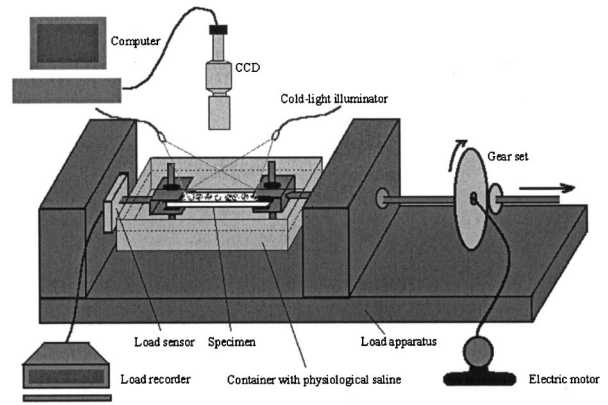


Fig. 3 Schematic of the deformation measurement system for DSCM.

$$\phi'(x, y, t_k) = \arccos \left[ \frac{I'(x, y, t_k) - I_0(x, y)}{I_m(x, y)} \right] \quad k = 1, 2, 3, \dots, n, \quad (16)$$

where

$$I_0(x, y) = \sum_{k=0}^n \frac{I'(x, y, t_k)}{n}, \quad I_m(x, y) = I'_{\max}(x, y) - I_0(x, y),$$

and  $I'_{\max}(x, y)$  is the maximum intensity value of the  $(x, y)$  position of all the  $I'(x, y, t_k)$  with  $k = 0, 1, 2, \dots, n$ .

The real phase  $\phi(x, y, t_k)$  can then be obtained by unwrapping the theoretical phase value<sup>28</sup>  $\phi'(x, y, t_k)$  and the strain can be obtained by

$$d = \frac{\lambda}{4 \pi \sin \theta} \Delta \phi \quad \text{and} \quad \mathbf{E}(\mathbf{r}) = [\partial d / \partial x \quad \partial d / \partial y]^T, \quad (17)$$

where  $d$  is the in-plane displacement,  $\theta$  is the angle between the illuminating and view directions,  $\lambda$  is the laser wavelength, and  $\mathbf{E}(\mathbf{r})$  is the corresponding strain distribution.

## 3 Experiment

### 3.1 Monoaxial Tensile Experiment of Cartilage Tissue Using DSCM

The articular cartilage was obtained from an intravital porcine, removed from adherent muscle tissues and cut from a near planar part into a rectangular test piece (Fig. 1). The specimen was sprayed with very minute water-insoluble black paint on its surface (Fig. 2), put into a container with physiological (0.9%) saline solution to maintain the necessary humidity, and then attached to a motor-driven monoaxis loading instrument (Fig. 3). To fix the specimen firmly, the clamping chucks were designed to be adjustable through bolting, and two pieces of raw emery papers were padded between the specimen and the chucks to reduce the direct damage to the specimen by metal as low as possible. The monoaxial tensile experiment was performed quasistatically at room temperature (18°C) with the loading speed of 0.04 mm/15 s. Finally, speckle patterns were captured by a CCD under white light and digitized by a frame grabber with the resolution of 59.56

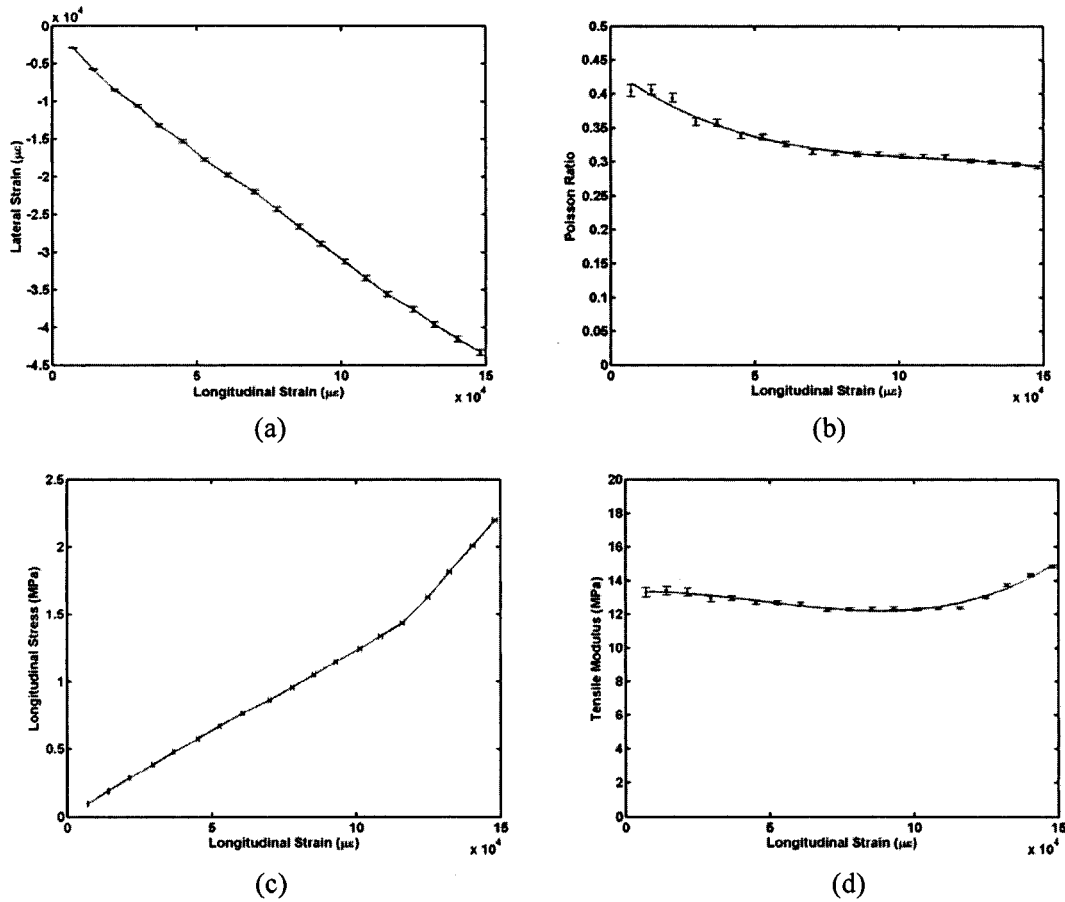


Fig. 4 Relationship curves for (a) lateral strain, (b) poisson ratio, (c) longitudinal stress, and (d) tensile modulus relative to longitudinal strain, respectively.

pixels/mm and an 8-bit pixel depth, and the tensile force was recorded synchronistically by a smart sensor with the sensitivity of 1.63N.

For the quasistatic loading experiment in this study, the displacement between two successive states is almost sub-pixel magnitude and can be determined by the gradient-based method directly without integer-pixel tracking. Moreover, with the series of speckle patterns, only the relative strain of the  $i$ 'th speckle pattern to the  $(i - 1)$ 'th speckle pattern must be determined by Eq. (12). The absolute strain of the  $i$ 'th speckle pattern is deduced based on the known relative strain by

$$\epsilon_i = \epsilon_{i-1} + e_j(1 + \epsilon_{i-1}) \quad i = 1, 2, \dots, n, \quad (18)$$

where  $\epsilon$  represents the absolute strain with  $\epsilon_0 = 0$ , and  $e$  means the relative strain.

Two mechanical parameters, Poisson ratio and tensile modulus, are extracted by the following equations

$$\mu_i = \frac{\epsilon_{iy}}{\epsilon_{ix}} \quad \text{and} \quad E_i = \frac{\sigma_i}{\epsilon_{ix}}, \quad (19)$$

relative to the  $i$ 'th speckle pattern,  $\mu_i$  and  $E_i$  are the Poisson ratio and the tensile modulus,  $\epsilon_{ix}$  and  $\epsilon_{iy}$  are the longitudinal strain (parallel to the tensile direction) and lateral strain (normal to the tensile direction), and  $\sigma_i$  is the longitudinal stress.

The results of longitudinal strain, lateral strain, Poisson ratio, longitudinal stress, and tensile modulus are presented in Fig. 4. Generally, the strain-stress plot shows linear relationship, which reflects the fact that the deformation of the specimen is elastic. The values of Poisson ratios fall in the 0.3 to 0.4 range and partly in the range of 0.36 to 0.5 mentioned in some connective work.<sup>29-31</sup> Compared with the tensile modulus, we obtained ranges from 12.3 to 14.85 MPa. A simple summary of the tensile moduli of cartilaginous tissues<sup>32-37</sup> is given in Table 1, which shows a different range of the tensile data distribution for each cartilage type.

### 3.2 Monoaxial Tensile Experiment of Vessel Tissue Using TSESPI

The inferior vena cava of a rabbit was preserved in the physiological (0.9%) saline solution after being extracted and used as the specimen in the monoaxial tensile experiment. The same loading instrument was used to attach the specimen after the container was removed. Soft emery papers were also padded into surfaces between the specimen and the grips to reduce the direct damage.

Note that it is very difficult to obtain the total precise dimensions for some soft tissues such as blood vessels, nerves, and tendons *in vivo*. It remains difficult to determine the original state the same as *in vivo* of such soft tissues and to measure the 3-D dimensions, especially the thickness, during *in*

**Table 1** Tensile moduli of cartilaginous tissues.

Tissue	Modulus	Refs.
Bovine articular cartilage	2–2.6MPa	Woo et al. <sup>32</sup>
Human articular cartilage	1–20 MPa	Akizuki et al. <sup>33</sup>
Human articular cartilage	0.68–12.49 MPa	Huang et al. <sup>34</sup>
Canine articular cartilage	26 MPa	Narmoneva et al. <sup>35</sup>
Porcine articular cartilage	18.0–19.5 MPa	Chae et al. <sup>36</sup>
Articular cartilages	1–43 MPa	Mow and Ratcliffe <sup>37</sup>

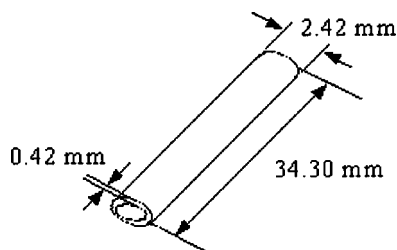
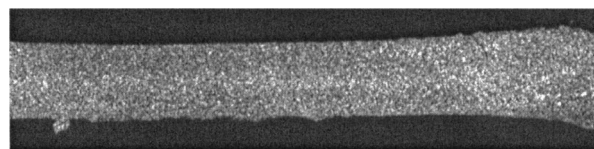
*in vitro* experiments. In this study, we assumed that the original zero-strain condition for the vessel was the condition when the force recorded by the smart sensor changed from zero. The thickness was the mean value measured in different positions when the specimen was dissected along the longitudinal direction after the experiment. The corresponding transverse section was supposed to be an annulus shape (Fig. 5).

The surface of the vessel was wetted with physiological saline solution in the time prior to subsequent experiments. During loading, 5000 frames of the speckle patterns (Fig. 6) were captured by a CCD with a speed of 25 frames/s and then digitized by a frame grabber with a resolution of 35.54 pixels/mm. On the other hand, the load recorder was placed in a dark box and illuminated by a spotlight, and a total of 13 frames of the load readings were captured and digitized by another set of CCD and frame grabber with a speed of 1 frame per 15 s. The two data acquisition systems work synchronistically. A very smart sensor with the sensitivity of 1g was introduced in the tensile experiment. Finally, the strain filed was obtained by Eq. (17) with  $\lambda=560$  nm and  $\theta=0.6608$  rad. A schematic of the deformation measurement system for TSESPi is shown in Fig. 7.

Figure 8 shows the results for stress versus strain and modulus versus force of the vessel. During the linear and elastic deformation of the specimen, the tensile moduli range from 4.8 to 5.9 MPa, which is higher than that of 1 MPa (Riley et al.<sup>38</sup>) and 2.4 MPa (Stein et al.<sup>39</sup>) in vascular tissues measurements.

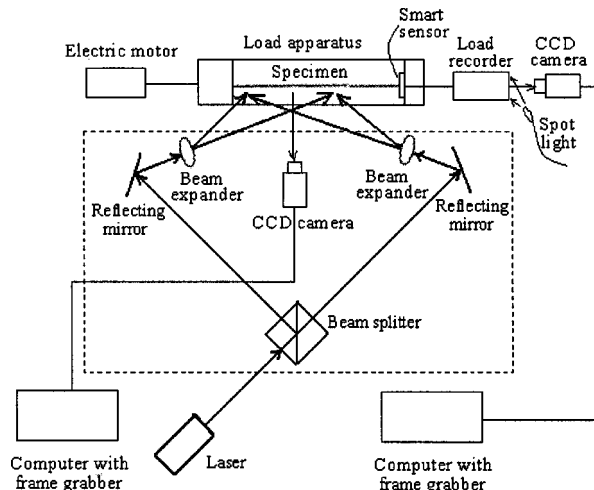
#### 4 Discussion and Conclusion

Digital speckle methods, such as the white light speckle method and the laser interference speckle method described in this work, were used to enable the special advantages of op-

**Fig. 5** Specimen dimensions between clamps.**Fig. 6** Specimen surface with speckles under laser interference.

tical inspection to be combined with equipment to try and overcome some traditional problems in the strain measurement of soft tissues. For speckle metrology, high data densities become available due to the possibility of generating very small scale speckles through manmade or laser interference, which make it possible to obtain the speckle patterns with a very high spatial resolution. Moreover, the rapid development of computer techniques has made it much easier to transfer the quantitative information into the computer memory when speckle patterns are observed with standard CCD cameras. Direct optical data capture, input, and analysis open the way to the storage of a large amount of experimental information and further make real-time measurement possible.

The DSCM technique has quickly developed during the last decade. Utilizing features of its easy test setup and low dependence on the environment, it is convenient to combine it with a microscope or a scanning electron microscope for the micro-object operation even in nanometer-scale measurement, which can greatly improve the accuracy of measurement, to some extent on the basis of the very high resolution of speckle patterns. The gradient-based algorithm for DSCM in this paper, with which only the first-order partial derivatives of the given functional are required to be calculated in a subset region, is more suitable for subpixel registration measurement with a sensitivity higher than 0.01 pixel, and the computational cost is far less than interpolation or differential iteration methods. Moreover, for the quasistatic deformation measurement, the final deformation can be obtained based on the superposition of tiny deformations of successive states by this technique instead of being calculated directly; therefore, the decorrelation caused by large deformations is avoided. Compared to DSCM, the interferometric technique ESPI has strin-

**Fig. 7** Schematic of the deformation measurement system for TSESPi.

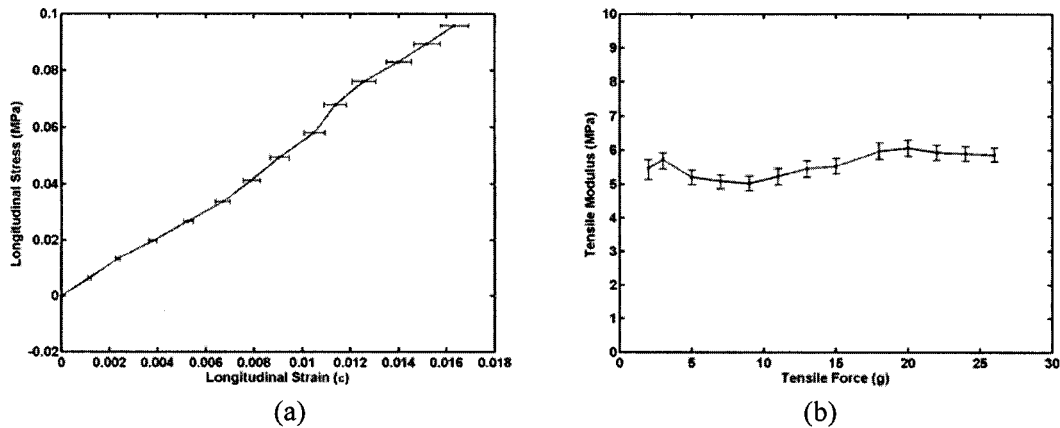


Fig. 8 Relationship curves for (a) stress versus strain and (b) tensile modulus versus tensile force.

gent requirements for system stability. The measuring range is fixed on the laser wavelength level (using a HeNe laser,  $\lambda=0.6328 \mu\text{m}$ ). The extended TSESPi technique, which is actually a kind of “time-carrier” technique where the carrier can be introduced by the consecutive object deformation instead of changing the angle between the object beam and the reference beam. It can be used to evaluate the phase map directly and further determine the continual deformations based on a temporal series of speckle patterns without phase shifting or tedious fringe analysis. When using this technique, a high-speed digital camera is recommended and enough frames of speckle patterns must be grabbed to ensure obtaining enough information for the temporal unwrapping. In addition, the total displacement measured by TSESPi is much greater than that obtained using conventional ESPI with the same testing system, and a displacement as small as half of a wavelength of the laser beam can also be resolved.

Employing the DSCM and TSESPi techniques, we extracted the mechanical behaviors (Poisson ratio and tensile modulus) of typical tissues based on noninvasive strain measurements. In the monoaxial tensile experiments for the cartilage tissue deformation ranging from 0 to 15%, values of the average error were found to be 0.052 to 2.5% of obtained strains. The corresponding parameters of mechanical behaviors are extracted based on the strain information, where the Poisson ratios are in the range of 0.3 to  $0.4 \pm 2.34\%$ , and the tensile moduli fall are from 12.3 to  $14.85 \pm 1.88\%$  MPa. On the other hand, based on the strains ranging from 0 to 0.017 with the average errors from 2.8 to 6.7% for the vessel measurement, the obtained tensile moduli fall are 4.8 to  $5.9 \text{ MPa} \pm 3.5$  to 6.3%. Overall, zero strain definition, local distortion of specimens, and random noises can be considered to be the major contributions to the measurement errors, while the system errors generated by the heavy dependence on the system’s stability in ESPI is one of the main reasons for the higher error. Nevertheless, the majority of measured values with errors less than 5% can reasonably be acceptable. In addition, since cartilaginous and vascular tissues always show instantaneous mechanical behaviors during testing due to their viscoelastic nature and different cell types and test portions, it is difficult to make a direct comparison with some results in the literature. However, these tensile findings suggest the similarities and differences between species and provide more infor-

mation for the design criteria and validation of tissue engineering attempts.

There is no doubt that many problems remain to be solved in this work on the strain measurement of soft tissues using speckle techniques. First, the effect of paints or dyes on the mechanical properties of the tissues has not been assessed, although it is normally necessary to mark the specimens in some way when using an optical method to monitor movement. Second, since standard mechanical extensometers or clamps usually have sharp spring-loaded knife edges to grip the specimen and may typically slice soft tissues, the clamping chucks we utilized were designed as of a bolt-loaded and rough rectangular interface holder. Nevertheless, clamping artifacts will still damage tissues and induce high strains in the grip zones during loading. Although only the midsubstance strains were measured for the derivation of meaningful mechanical properties, the necessity of lessening the disadvantages caused by the local distortion of the test piece was reinforced. In addition, the experiments revealed the fundamental difficulty of defining zero strain in such prestressed and viscoelastic tissues; different definitions will lead to different results for the strain measurement. How to avoid strains to be measured relative to an arbitrarily defined zero strain for tissue becomes more and more important, which has not been of great concern to date in *in vitro* measurements.

Until now, most of the experiments on living tissues are performed *in vitro* due to the lack of reliable noninvasive techniques for a direct *in vivo* strain measurement. For the two speckle methods themselves, however, there is no limitation to *in vivo* measurement. Under certain conditions, the fiber technique combined with DSCM may be a better choice for *in vivo* testing. The correlation operation of the speckle images extracted by optical fibers at different times or under different conditions may make it possible to obtain more accurate and useful information, which shows promise in future *in vivo* measurement. A relative experiment is in progress.

#### Acknowledgments

The authors would like to acknowledge the National Natural Science Foundation of China (NSFC) Grant No. 19972033 and the Tsinghua University Fund Grant No. GC 2001031 for this research work.

## References

1. Y. C. Fung, *Biomechanics: Motion, Flow, Stress, and Growth*, Springer-Verlag, New York (1990).
2. H. Yamada, *Strength of Biological Materials*, Baltimore, MD (1970).
3. F. J. Carter, "Biomechanical testing of intra-abdominal soft tissue," in *Proc. Intl. Workshop on Soft Tissue Deformation and Tissue Palpation*, Cambridge (1998).
4. N. Abraham Cohn, S. Y. Emelianov, M. A. Lubinski, and M. O'Donnell, "An elasticity microscope. Part I: methods," *IEEE Trans. Ferroelect. Freq. Control* **44**, 1304–1319 (1997).
5. S. Arms, J. Boyle, R. Johnson, and M. Pope, "Strain measurement in the medical collateral ligament of the human knee: an autopsy study," *J. Biomech.* **16**(7), 491–496 (1983).
6. J. G. Howe, C. Wertheimer, and R. J. Johnson, "Arthroscopic strain gauge measurement of the normal anterior cruciate ligament," *J. Arthrosc. Rel. Surg.* **6**(3), 198–204 (1990).
7. R. Pietrabissa, L. Gionso, V. Quaglini, E. Di Martino, and M. Simion, "An in vitro study on compensation of mismatch of screw versus cement-retained implant supported fixed prosthesis," *Clin. Oral Implants Res.* **11**, 448–457 (2000).
8. C. J. Wang, P. S. Walker, and B. Wolf, "The effects of flexion and rotation on the length patterns of the ligaments of knee," *J. Biomech.* **6**, 587–596 (1973).
9. D. L. Bartel, J. L. Marshall, R. A. Schieck, and J. B. Wang, "Surgical repositioning of the medial collateral ligament," *J. Bone Joint Surg. Br.* **59A**(1), 107–116 (1977).
10. P. C. Amadio, L. J. Berglund, and K. N. An, "Biochemically discrete zones of canine flexor tendon: evaluation of properties with a new photographic method," *J. Orthop. Res.* **10**(2), 198–204 (1992).
11. D. L. Butler, M. Y. Sheh, and D. C. Stouffer, "Surface strain variation in human patellar tendon and knee cruciate ligaments," *J. Biomech. Eng.* **112**, 38–45 (1990).
12. N. Yamamoto, K. Hayashi, and H. Kuriyama, "Mechanical properties of the rabbit patellar tendon," *J. Biomech. Eng.* **114**, 332–337 (1992).
13. G. A. Johnson, D. M. Tramaglini, and R. E. Levine, "Tensile and viscoelastic properties of human patellar tendon," *J. Orthop. Res.* **12**(6), 796–803 (1994).
14. M. K. Smolek, "Holographic interferometry of intact and radially incised human eye-bank corneas," *J. Cataract Refractive Surg.* **20**, 277–286 (1994).
15. J. F. Orr and J. C. Shelton, *Optical Measurement Methods in Biomechanics*, Chapman & Hall, London (1997).
16. S. L.-Y. Woo, C. Orlando, J. Camp, and W. Akeson, "Effects of post-mortem storage by freezing on ligament tensile behavior," *J. Biomech.* **19**, 399–404 (1986).
17. M. Runza, R. Pietrabissa, S. Mantero, and A. Albani, "Lumbar dura mater biomechanics: experimental characterization and scanning electron microscopy observations," *Anesth. Analg. (Baltimore)* **88**, 1317–1321 (1999).
18. F. Lauper, "Mesures et modélisation des effets de la viscosité à mémoire longue du ligament croisé antérieur," Diplôme d'ingénieur physicien, EPFL (1996).
19. R. C. Haut and R. C. Powlison, "The effects of test environment and cyclic stretching on the failure properties of human patellar tendons," *J. Orthop. Res.* **8**, 532–540 (1990).
20. Y. C. Fung, *Biomechanics: Mechanical Properties of Living Tissues*, 2nd ed., Springer-Verlag (1993).
21. W. H. Peters and W. F. Ranson, "Digital imaging technique in experimental stress analysis," *Opt. Eng.* **21**(3), 427–431 (1982).
22. G. C. Jin, N. K. Bao, and P. S. Chung, "An advanced digital speckle correlation method for strain measurement and nondestructive testing," *Proc. SPIE* **2921**, 572–577 (1996).
23. Y. C. Chan, X. Dai, G. C. Jin, N. K. Bao, and P. S. Chung, "Nondestructive detection of delaminations in multilayer ceramic capacitors using improved digital speckle correlation method," *Microwave Opt. Technol. Lett.* **16**, 80–85 (1997).
24. A. Makovski, "Time lapse interferometry and confounding using television system," *Appl. Opt.* **10**(12), 2722–2730 (1971).
25. L. Ole, "Electronic speckle pattern interferometry," *Phys. Technol.* **11**, 16–22 (1980).
26. N. K. Bao, G. C. Jin, and P. S. Chung, "A new electronic shearing speckle pattern interferometry with continuously variable sensitivity," *Proc. SPIE* **2066**, 63–66 (1993).
27. J. Zhang, G. C. Jin, S. P. Ma, and L. B. Meng, "Application of an improved subpixel registration algorithm on digital speckle correlation measurement," *Opt. Laser Technol.* **35**(7), 533–542 (2003).
28. X. D. Li, G. Tao, and Y. Z. Yang, "Continual deformation analysis with scanning phase method and time sequence phase method in temporal speckle pattern interferometry," *Opt. Laser Technol.* **33**, 53–59 (2001).
29. D. H. Hoch, A. J. Grodzinsky, T. J. Koob, M. L. Albert, and D. R. Eyre, "Early changes in the material properties of rabbit articular cartilage after meniscectomy," *J. Orthop. Res.* **1**, 4–12 (1983).
30. R. D. Altman, J. Tenenbaum, L. Latta, W. Riskin, L. N. Blanco, and D. S. Howell, "Biomechanical and biochemical properties of dog cartilage in experimentally induced osteoarthritis," *Ann. Rheum. Dis.* **43**, 83–90 (1984).
31. J. Jurvelin, I. Kiviranta, J. Arokoski, M. Tammi, and H. J. Helminen, "Indentation study of the biomechanical properties of articular cartilage in the canine knee," *Eng. Med.* **16**, 15–22 (1987).
32. S. L. Woo, W. H. Akeson, and G. F. Jemmott, "Measurements of nonhomogeneous, directional mechanical properties of articular cartilage in tension," *J. Biomech.* **9**, 785–791 (1976).
33. S. Akizuki, V. C. Mow, F. Muller, J. C. Pita, D. S. Howell, and D. H. Maticourt, "Tensile properties of human knee joint cartilage: I. Influence of ionic conditions, weight bearing, and fibrillation on the tensile modulus," *J. Orthop. Res.* **4**, 379–392 (1986).
34. C. Y. Huang, S. D. Matthews, R. G. Pollock, R. J. Pawluk, E. L. Flatow, L. U. Bigliani, and V. C. Mow, "Regional and directional tensile properties of bovine glenohumeral cartilage," *Adv. Bioeng.* **35**, 525–526 (1997).
35. D. A. Narmoneva, J. Y. Wang, and L. A. Setton, "Nonuniform swelling-induced residual strains in articular cartilage," *J. Biomech.* **32**, 401–408 (1999).
36. Y. S. Chae, G. Aguilar, E. J. Lavernia, and B. J. F. Wong, "Characterization of temperature dependent mechanical behavior of cartilage," *Lasers Surg. Med.* **32**, 271–278 (2003).
37. V. C. Mow and A. Ratcliffe, *Basic Orthopaedic Biomechanics*, Lippincott-Raven, Philadelphia (1997).
38. W. A. Riley, R. W. Barnes, G. W. Evans, and G. L. Burke, "Ultrasonic measurement of the elastic modulus of the common carotid artery: the Atherosclerosis Risk in Communities (ARIC) Study," *Stroke* **23**, 952–956 (1992).
39. P. D. Stein, M. S. Harnid, K. Shivkumar, T. P. Davis, T. Khaja, and J. W. Henry, "Effects of cyclic flexion of coronary arteries on progression of atherosclerosis," *Am. J. Cardiol.* **73**, 431–437 (1994).